Tellus (1999), 51A, 922–936
Printed in UK – all rights reserved



TELLUS
ISSN 0280–6495

# Spatial characteristics of the tropical cloud systems: comparison between model simulation and satellite observations

By GUANG J. ZHANG[1]*, DANCE ZUROVAC-JEVTIC[2] and ERWIN R. BOER[3]†, [1]*Center for Atmospheric Sciences, Scripps Institution of Oceanography, La Jolla, CA 92093-0221, USA;* [2]*Department of Meteorology, Stockholm University, S-106 91 Stockholm, Sweden;* [3]*Center for Clouds, Chemistry and Climate, Scripps Institution of Oceanography, La Jolla, CA 92093-0221, USA*

(Manuscript received 15 September 1998; in final form 2 March 1999)

ABSTRACT

A Lagrangian cloud classification algorithm is applied to the cloud fields in the tropical Pacific simulated by a high-resolution regional atmospheric model. The purpose of this work is to assess the model's ability to reproduce the observed spatial characteristics of the tropical cloud systems. The cloud systems are broadly grouped into three categories: deep clouds, mid-level clouds and low clouds. The deep clouds are further divided into mesoscale convective systems and non-mesoscale convective systems. It is shown that the model is able to simulate the total cloud cover for each category reasonably well. However, when the cloud cover is broken down into contributions from cloud systems of different sizes, it is shown that the simulated cloud size distribution is biased toward large cloud systems, with contribution from relatively small cloud systems significantly under-represented in the model for both deep and mid-level clouds. The number distribution and area contribution to the cloud cover from mesoscale convective systems are very well simulated compared to the satellite observations, so are low clouds as well. The dependence of the cloud physical properties on cloud scale is examined. It is found that cloud liquid water path, rainfall, and ocean surface sensible and latent heat fluxes have a clear dependence on cloud types and scale. This is of particular interest to studies of the cloud effects on surface energy budget and hydrological cycle. The diurnal variation of the cloud population and area is also examined. The model exhibits a varying degree of success in simulating the diurnal variation of the cloud number and area. The observed early morning maximum cloud cover in deep convective cloud systems is qualitatively simulated. However, the afternoon secondary maximum is missing in the model simulation. The diurnal variation of the tropospheric temperature is well reproduced by the model while simulation of the diurnal variation of the moisture field is poor. The implication of this comparison between model simulation and observations on cloud parameterization is discussed.

## 1. Introduction

The spatial and temporal characteristics of clouds are important climatic parameters. Recently, Boer and Ramanathan (1997) (hereafter referred to as BR) developed an algorithm to determine these cloud characteristics from the satellite data over the tropical western and central Pacific. They found that over 95% of the radiatively important clouds are of scales resolvable by GCMs with a horizontal resolution of about 50 km. They also examined the scale dependence of the cloud physical and radiative properties for

* Corresponding author.
e-mail: gzhang@ucsd.edu
† Additional affiliation: Nissan Cambridge Basic Research, Cambridge, Massachusetts.

various cloud types. Their study provides a new approach to validating and improving cloud parameterization in global and regional climate models.

Validation of cloud simulation in GCMs and regional models is often performed by comparing the geographic distribution of the time-averaged fields with the observations (Del Genio et al., 1996; Karlsson, 1996; Yu et al., 1997). While this approach is useful for diagnosing the deficiency in the simulated cloud climatology with respect to geographic locations, it cannot relate the deficiency to a specific cloud type. Since different physical processes are involved in the formation and maintenance of different cloud types, the traditional approach offers little for improvement in cloud parameterization except over regions where a particular type of clouds are prevalent. On the other hand, the Lagrangian approach of BR examines clouds by their types and spatial scales. When this approach is applied to the simulated cloud fields and compared with the observations, it will enable one to evaluate the simulation of the individual types and spatial scales of clouds, regardless of their location. Thus, it would be possible to relate the simulation deficiency to that of the representation of the physical processes responsible for the particular cloud types.

In this study, we will apply BR's approach to the cloud fields simulated by a regional atmospheric model and compare the spatial characteristics of the model clouds with those from the satellite observations. All satellite observations shown in this paper are taken from BR. Section 2 of this paper will describe the model used in this study and the simulation of the cloud systems. Section 3 presents the analysis method. The main results will be presented in Section 4. Section 5 will summarize the main results and present some discussions on the implication of the model results for cloud parameterization.

## 2. Model and simulation of the cloud systems

The model used for this study is the Stockholm University version of the HIgh Resolution Limited Area Model (HIRLAM). It is a primitive equation weather forecasting model developed by the HIRLAM project involving a number of Nordic and other European countries. The dynamic framework of the model is based on the ECMWF regional gridpoint model. The model has 16 vertical levels in a hybrid coordinate system extending from the surface to 25 hPa, and a horizontal dimension of $110 \times 100$ gridpoints at a resolution of $0.5^\circ$ in latitude and longitude. The model has a comprehensive physical parameterization package. The boundary layer processes are parameterized following Louis (1979). The short-wave and long-wave radiation as well as the cloud radiative effects are parameterized following Savijärvi (1991). Of particular interest to this study is the cloud parameterization, which uses the prognostic cloud water parameterization scheme developed by Sundqvist et al. (1989). This cloud parameterization scheme has been used in various forms by many GCM groups worldwide. Several studies have documented the performance of the HIRLAM model. Huang and Sundqvist (1993) evaluated the use of initialization of cloud water content and cloud cover in the improvement of the model forecasts. Karlsson (1996) evaluated the simulation of the cloud distribution in the Nordic region.

In this study, the model is run over the tropical western and central Pacific, covering (155°E, 150°W) and (30°S, 20°N). The period of simulation is 30 days from 7 March to 5 April 1993. Since HIRLAM is a forecast model, we perform a 36-h forecast for each of the 30 days starting from 00 GMT. To allow for model spin-up the first 12 h model output is discarded and only the last 24-h data are used to represent the simulation day. The data are saved every 6 h. The analyzed atmospheric fields and sea surface temperature from ECMWF are used for the model's initial and lateral boundary conditions.

The size distribution of the simulated clouds is determined using the cloud classification algorithm of BR, with the cloud top temperature and the fractional cloud cover as input. BR used effective brightness temperature as input to their algorithm. Since the model does not have this variable, we use the cloud top temperature instead. According to Liu et al. (1995), brightness temperature $T_e$ and loud top temperature $T_c$ may be related by the following approximate expression:

$$T_c = T_e + 8(T_e/150 - 1).$$

This expression cannot be applied near the cloud edge, where the optical depth is such that $T_e$ no longer represents the cloud top temperature, but is a measure of the combined effect of radiation from the cloud itself, the column of air below the cloud and the surface. Due to the approximate nature of this relationship, we will not use it to convert model output $T_c$ to $T_e$. Instead, we will use it to estimate the $T_c$ bounds for each cloud type, so that the cloud types have approximately the same $T_e$ bounds as used in BR. Due to the relatively coarse vertical resolution of the model, the clouds are divided into three categories: deep convective systems with cloud top temperature less than 235 K, mid-level clouds with cloud top temperature between 235 K and 275 K, and low clouds with cloud top temperature greater than 275 K. The deep clouds roughly correspond to those with cloud tops above 300 hPa, the mid-level clouds have their tops between 600 hPa and 300 hPa, and the low clouds have their tops below the 600 hPa level. Within the deep cloud category, the cloud systems are further divided into mesoscale convective systems (MCS) and non-mesoscale systems (non-MCS) using the criterion set by BR. To be classified as an MCS, a cloud must have a core with the cloud top temperature less than 219 K and an area greater than $5 \times 10^4$ km$^2$. The core must be surrounded by anvils with cloud top temperature less than 240 K, and the area of the core plus anvils must exceed $10^5$ km$^2$. The deep cloud systems that do not belong to MCS are classified as non-MCS.

## 3. Analysis method

To evaluate the model's ability to reproduce satellite observed cloud spatial characteristics, we extended the Detect-And-Spread (DAS) algorithm of BR to accommodate the issues particular to our low (0.5° in both latitude and longitude) model resolution. BR used GMS satellite observations registered at approximately 0.05° resolution. Furthermore, the original DAS operated on the effective brightness temperature field $T_e$, which is not available from our model. The primary reason for using $T_e$ in the original cloud segmentation, besides its diurnal availability, was the fact that $T_e$ increases as a cloud's optical depth decreases towards its perimeter. This characteristic was used to break apparently attached clouds apart. Therefore, we devised a method to generate a geometric temperature field ($T_g$) that also shows an increase towards the edges of cloudy regions, and use it as input to our DAS.

We first briefly discuss DAS as presented in BR, followed by a discussion of the changes we made. Cloud segmentation in DAS consists of a multi-stage process. It first detects cores of very cold clouds (i.e., $T_e < T_{d1}$). A core is defined as a set of pixels whose temperature is less than a particular value and are connected via pixels that also satisfy this temperature criterion. Then it grows each core by adding adjacent pixels whose temperature is "close" (i.e., $T_e < T_{s1} > T_{d1}$). In a three-step iterative process it spreads each core out a little at a time to prevent one core's edge from wrapping around another core. Subsequently it enters the second detect stage in which it finds cores whose temperature is warmer than $T_{d1}$ but colder than $T_{s1}$ (i.e., $T_e < T_{d2}$ where $T_{d1} < T_{d2} < T_{s1}$). The latter constraint is necessary to avoid new cloud cores being directly attached to already existing grown cores. Now it grows all new cores and already existing grown cores a little further until their edge reaches either the $T_{s2}$ contour or another grown core (i.e., $T_e < T_{s2}$). This process of detecting new cores and spreading all new and already existing grown cores is repeated until the desired maximum temperature is reached or all remaining pixels are either clear sky or already labeled. Upon completion, DAS produces cloud size distribution, average cloud area within each size bin, and the scale dependence of a number of cloud physical and radiative properties.

For model data, since the effective brightness temperature is not available, a geometric temperature field ($T_g$) is used to quantify our intuitive notion that cloudy regions that are similar in cloud top temperature but are connected only by a narrow pathway of cloudy pixels should be segmented into separate clouds. To generate $T_g$, the following algorithm is used. First, fractional cloud cover has to be converted to one possible realization of the underlying cloud field, assuring that the total cloud cover is preserved. This is accomplished by assigning complete cloud cover to every grid cell for which a random number generator generates a uniformly distributed number between zero and one that is less than the fractional cloud cover of that cell. This results in a binary cloud map. The binary cloud map is then converted to an Euclidian distance map (Russ, 1992) in which the values represent the distance of each non-zero grid cell to the nearest cloud edge; i.e., a cloud cell which has an adjacent cell (8-connected adjacency) with a zero. The distance is measured in terms of the minimum number of east–west plus north–south steps required to reach a cloud edge cell. Given that the model resolution is 0.5° in latitude and longitude, a distance of one corresponds to about 55 km around the equator.

The Euclidian distance map $D$ and the cloud top temperature $T_c$ are used as follows to compute $T_g$ for each grid cell:

$$T_g = \begin{cases} T_c & D > 3 \\ T_c + \dfrac{(3-D)}{2}(285 - T_c) & D \leqslant 3, \end{cases}$$

which means that $T_g$ approaches the clear sky brightness temperature (considered to be 285 K) at the cloud edge. This simple technique proves very effective for the intended cloud segmentation purpose. DAS then is applied to $T_g$ in a similar manner to BR. The distance limit of $D = 3$ from the cloud edge to modify $T_g$ is admittedly arbitrary. However, sensitivity tests with different values of $D$ suggest that the results of the cloud size distribution are not sensitive to it (use of larger $D$ gives slightly more smaller clouds).

## 4. Results

### 4.1. *Time-mean cloud statistics*

*4.1.1. Cloud distribution.* Fig. 1 shows the scatter plot of the monthly mean cloud cover between satellite observations and the model simulation. The cloud cover from satellite observations are obtained by dividing the area of cloudy pixels ($T_e < 285$ K) by the total area of each 0.5° × 0.5° grid cell collocated with the model grid cell. In general, there is a good agreement between the observed and simulated cloud cover. The slope of 1.05 with a correlation coefficient of 0.89 suggests that the model simulation of the total cloud cover is about 5% lower relatively and the model explains about 80% of the cloud cover variation. However, as we will see below, when the total simulated cloud cover is broken down into different cloud types and scales, the simulation deficiency of certain cloud types and scales becomes apparent.

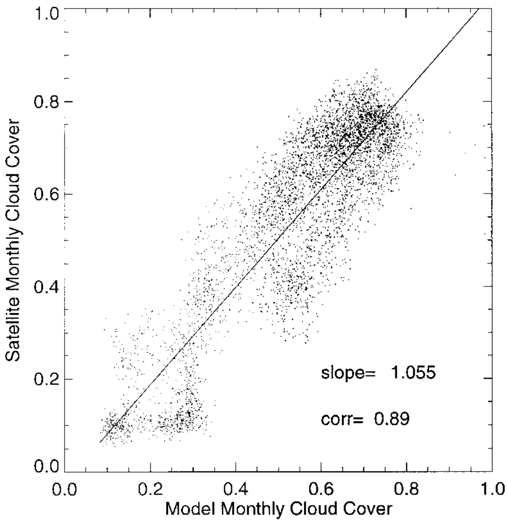


*Fig. 1.* Scatter plot of simulated versus observed total cloud cover averaged over the 30-day simulation period. The satellite observations are collocated with the model grid points.

Fig. 2 compares the cumulative distribution of the fractional cloud cover between the satellite observations and the model simulation for the three broadly grouped cloud types as defined in Section 2. The shaded areas represent the uncertainty scale due to the model resolution. The area contribution from the relatively smaller ($< 10^5$ km$^2$) deep convective cloud systems in the model is significantly less than observed. On the other hand, the total contribution to the cloud cover by the deep clouds of all sizes in the model is only slightly less than observed (23% versus 26%), suggesting that the modeled deep convective cloud systems are biased toward large cloud sizes. This may be partially due to the coarse vertical resolution of the model. For instance, the model would not be able to detect the cloud top variation within the thickness of a model layer, but the satellite would. Therefore, a few small clouds connected by shallow valleys may have been represented as one big cloud in the model. However, it is unlikely that the model resolution is responsible for the majority of the difference in the area contribution as functions of cloud size. Within the deep convective cloud systems, the cumulative contribution from MCSs to the fractional cloud

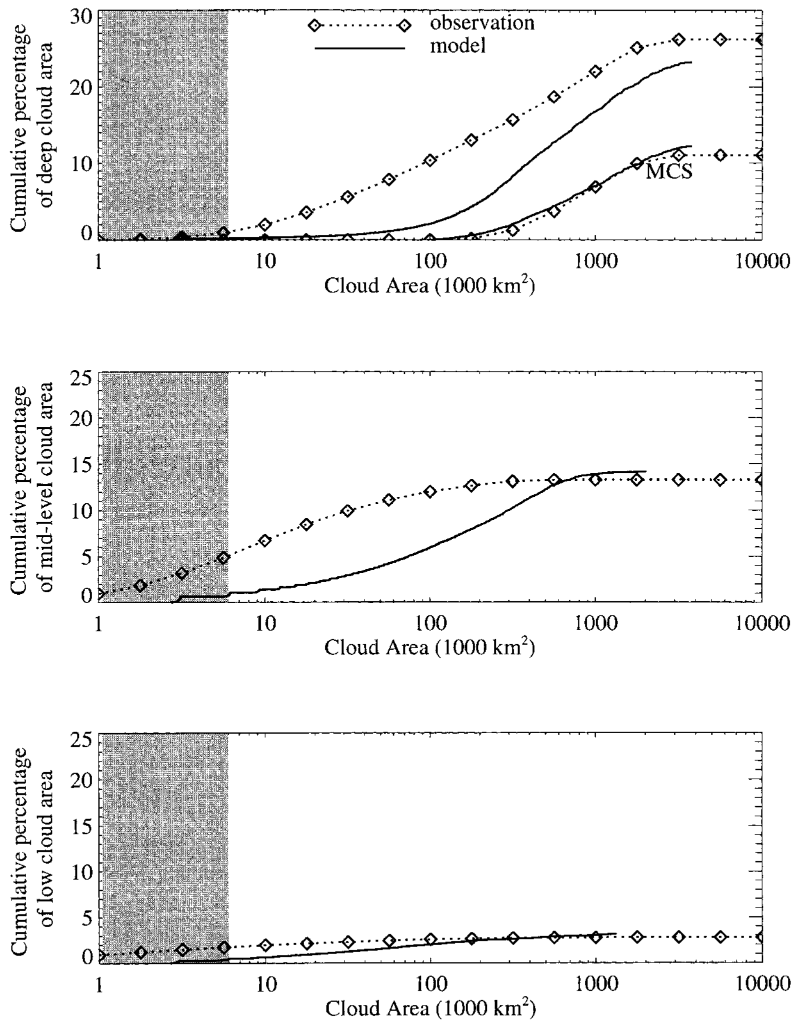


*Fig. 2.* Cumulative contribution from different cloud types to the total cloud cover as functions of the cloud area. The monthly mean total cloud cover is 42% from the satellite and 40% from the model.

area as a function of the cloud area is very well simulated compared to the observations. The cloud cover from MCSs accounts for slightly less than half of the total cloud cover from all deep cloud systems.

The simulation of the cumulative area contribution from the mid-level clouds is qualitatively similar to that of the deep clouds, that is, the contribution from the smaller cloud systems is under-simulated, with a bias toward larger cloud sizes. The total contribution from this cloud type of all sizes in the model is in good agreement with the observations. The cumulative contribution of the low-level clouds is also well simulated in the model. Most of the differences between the simulated and observed contributions are from the gridpoint scale clouds where large uncertainty exists. Due to the relatively small fractional cloud cover from this cloud type, the bias is not as significant as for the other two cloud types. Note that the contributions to the total fractional cloud cover from deep, mid-level, and low clouds in the model are 23%, 14% and 3%, respectively, yielding a total modeled fractional cloud cover of

40%. These numbers compare well with the observed values of 26%, 13% and 3%, respectively, for a total fractional cloud cover of 42%.

The number distribution of clouds as a function of cloud area for different cloud types is shown in Fig. 3. Consistent with the cloud cover, the model significantly under-simulates the number of clouds with area less than $10^5$ km$^2$ for deep convective systems and $3 \times 10^4$ km$^2$ for mid-level clouds. For larger cloud systems, the model performs much better. In general, clouds of relatively small sizes dominate the cloud number population for all cloud types, although large clouds account for a significant portion of the cloud cover. For instance, there are only a few MCSs per scene, but they account for almost half of the total deep cloud cover.

*4.1.2. Dependence on cloud type and scale.* Cloud physical and radiative properties strongly depend on the cloud types. Using satellite infrared and microwave data in the western Pacific, Liu et al. (1995) showed that precipitation and cloud liquid water path vary widely from one cloud type to

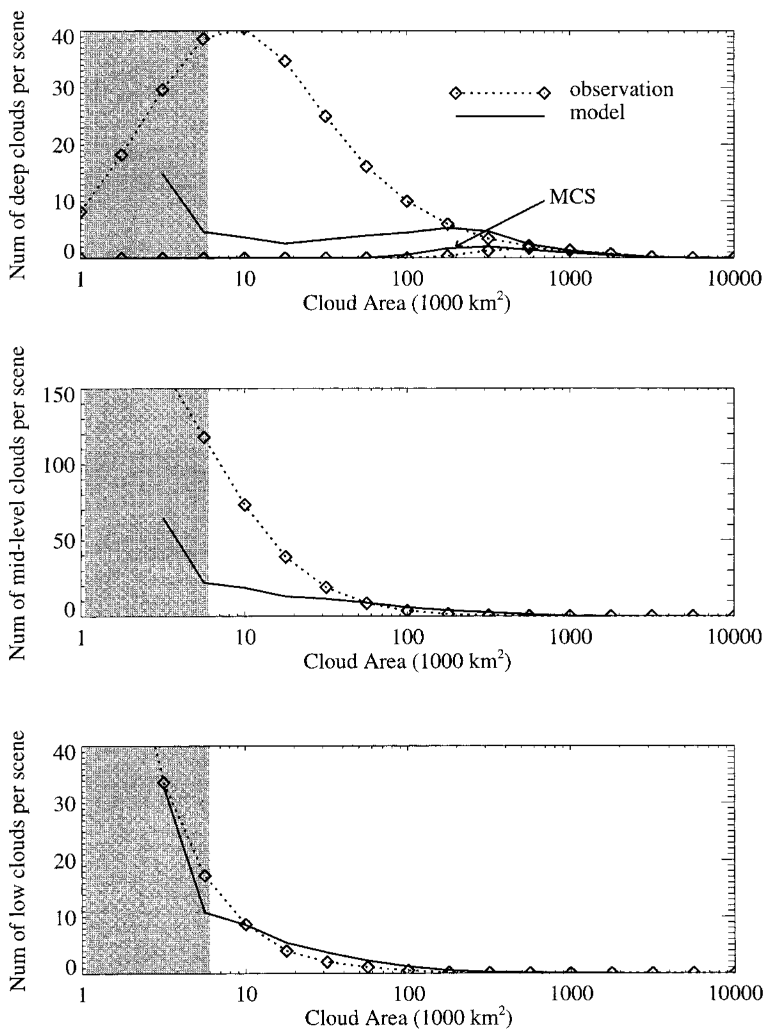


*Fig. 3.* Number distribution of different types of clouds as functions of their area. The dashed line is based on the satellite results of Boer and Ramanathan (1997).

another. Similar results are obtained in our model. Fig. 4 shows the cloud liquid water path and 6-h cumulative rainfall as functions of the cloud area and type from the model. Also shown are the surface sensible and latent heat fluxes underneath the cloud systems. While the association of precipitation and cloud liquid water path with cloud systems is intuitively obvious, the dependence of surface sensible and latent heat fluxes on cloud type and area is not as direct. However, note that cloud systems affect the large-scale circulation, which in turn affects the surface air–sea fluxes. The cloud liquid water path in deep and mid-level convective cloud systems increases with the cloud size for small clouds, then levels off and even decreases as cloud scale further increases. On the other hand, within the low-level clouds, the cloud liquid water path

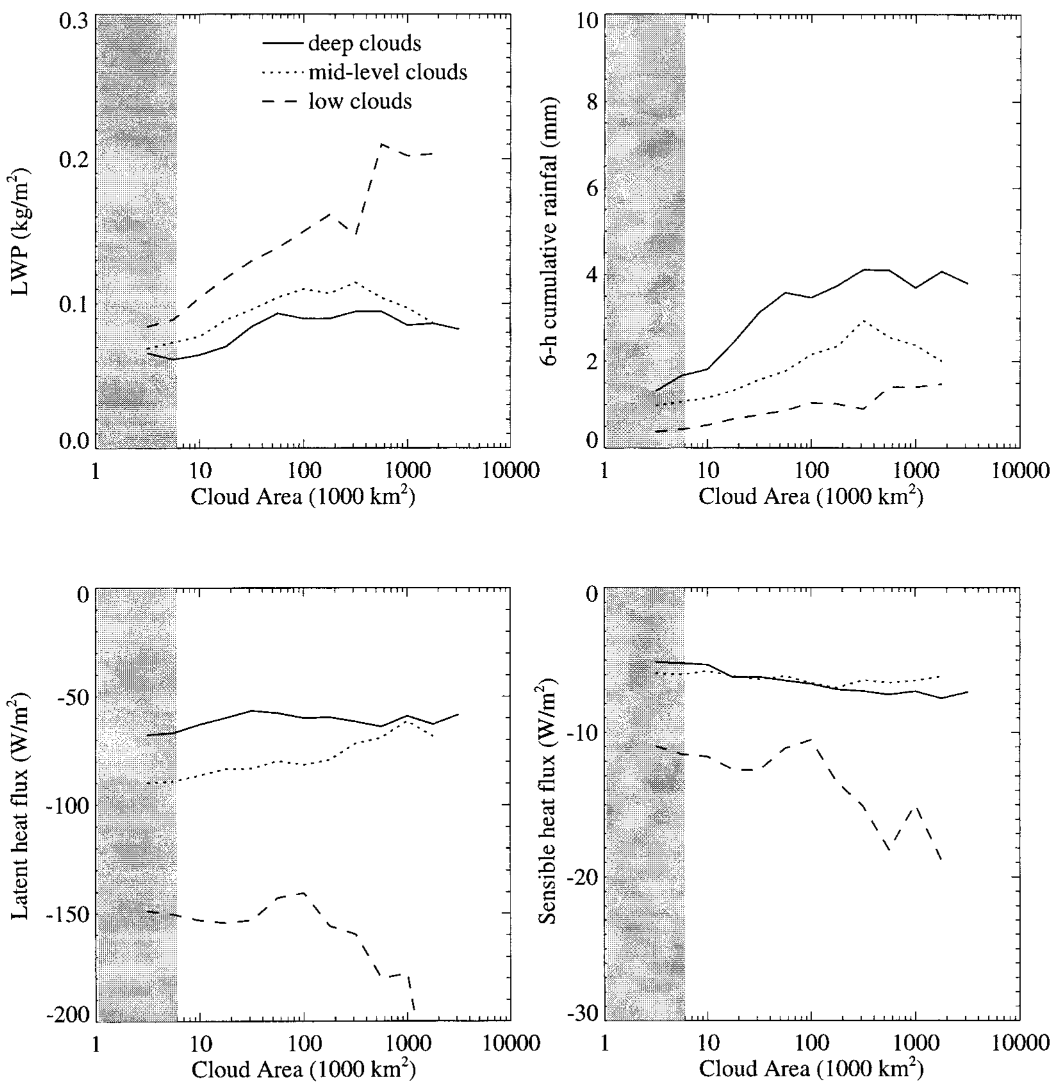


*Fig. 4.* Liquid water path, 6-h cumulative rainfall, surface latent and sensible heat fluxes as functions of the cloud area based on the model simulation.

increases with cloud area over the entire cloud size spectrum. The kinks are noises due to size binning and the fact that there are only very few large low level clouds. The cloud liquid water path is the largest for low-level clouds, and smallest for deep clouds, similar to the observations of Liu et al. (1995). The 6-h cumulative rainfall for low clouds increases with cloud area. But for mid-level and deep clouds it increases for small cloud size and then either levels off or decreases as the cloud scale further increases. At a given cloud scale, rainfall is heaviest in deep clouds and lightest in low clouds.

The dependence of the surface latent and sensible heat fluxes on cloud type and area is interesting. The latent heat flux under deep and mid-level clouds is relatively low and remains constant or decreases with cloud area. Under low clouds it is significantly higher, and remains roughly constant for smaller clouds, but increases considerably with cloud area for cloud areas $>10^5$ km$^2$. Similar features are seen for sensible heat flux. One possible reason is that low clouds often occur in the subtropical areas where surface winds are relatively strong compared to the equatorial convective regions. Another reason may be that large-scale convective regime tends to have weak surface winds and fluxes (Zhang et al., 1995).

To examine how the vertical motion and relative humidity in cloudy region depend on the scale of the convective systems, Fig. 5 shows the vertical velocity and relative humidity distribution as functions of the cloud area for MCS and non-MCS. The upward motion in MCSs has a broad maximum in the mid-troposphere from about 600 hPa to 300 hPa. In terms of scale dependence, maximum upward motion occurs inside MCSs of size close to $1000 \times 10^3$ km$^2$. In other words, giant supercluster type of MCSs do not necessarily have the strongest upward motion inside them. The relative humidity has a minimum in the mid-troposphere, and changes little with cloud area in both the middle and lower troposphere. In the upper troposphere, relative humidity reaches a maximum above 200 hPa in MCSs, and it increases with the cloud size. The intensity of upward motion inside non-MCSs is weaker than MCSs. The maximum occurs for cloud areas between 100 and $1000 \times 10^3$ km$^2$. The relative humidity distribution for large non-MCSs is similar to MCSs in that there is a minimum in the mid-troposphere and that relative humidity increases with the cloud area in the upper troposphere. For small convective cloud systems, say 10 to $100 \times 10^3$ km$^2$, the relative humidity increases with the cloud size, particularly in the upper troposphere.

Observational studies using satellite data (Rind et al., 1991; Sun and Lindzen, 1993; Soden and Fu, 1995) indicate that the upper tropospheric humidity in the tropics is closely associated with convection and clouds. Convective regions are moister than the suppressed regions. The model behaves in similar fashion. Fig. 6 shows the vertical profiles of cloud fraction, relative humidity and deviation of the specific humidity from the domain mean, stratified according to the vertical velocity at 600 hPa, which approximately measures the low-level mass convergence. A gridpoint is considered having upward motion if the vertical $p$-velocity $\omega < -0.15$ Pa/s, a descending region is defined with $\omega > 0.01$ Pa/s, and the transition region has the vertical velocity in between. The vertical velocity values used here are arbitrary, only for the purpose of qualitatively separating the upward motion region from the downward motion region within the model domain. The fractional cloud cover is the largest in ascending regions and smallest in subsidence region, with that in transition region falling in between. There are abundant low-level clouds as well as high clouds in the subsidence region. The low-level clouds may be from shallow convection under convectively suppressed conditions whereas the high-level clouds may be the extended anvils from the adjacent convective regions that can be an important source of water vapor in the subsidence region (Sun and Lindzen, 1993). The largest difference in relative humidity between different vertical velocity regimes is above the 800 hPa level. The atmosphere is moister in ascending regions than in the subsidence and transition regions. Despite the considerable difference in cloud cover between the subsidence regions and the transition regions, particularly in the middle troposphere, the relative humidity difference is small, consistent with the suggestion by Sun and Lindzen (1993) that the high clouds may serve as important moisture sources for the atmosphere below. In terms of specific humidity, the profiles of its deviation from the domain average show that the upward motion region is moister than

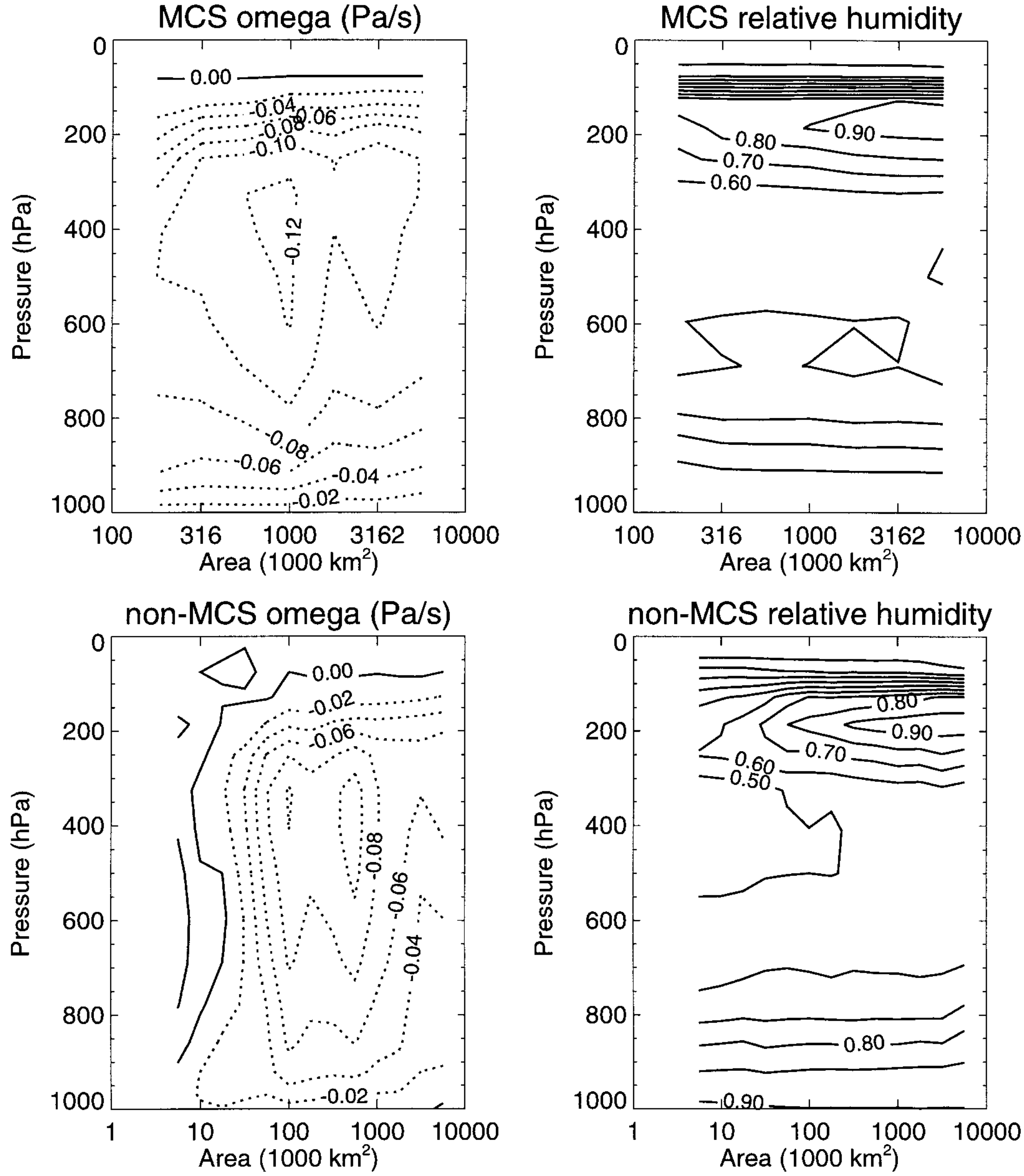


*Fig. 5.* Dependence of vertical velocity and relative humidity on cloud area for MCS and non-MCS deep convective cloud systems as simulated by the model.

the domain average while the subsidence region is drier. The transition region is about the same as the domain average except in the lower troposphere below 800 hPa where the transition region is drier.

*4.2. Diurnal variation*

There is a significant diurnal variation of convective activity in the western Pacific warm pool (Fu et al., 1990; Mapes and Houze, 1993; Chen

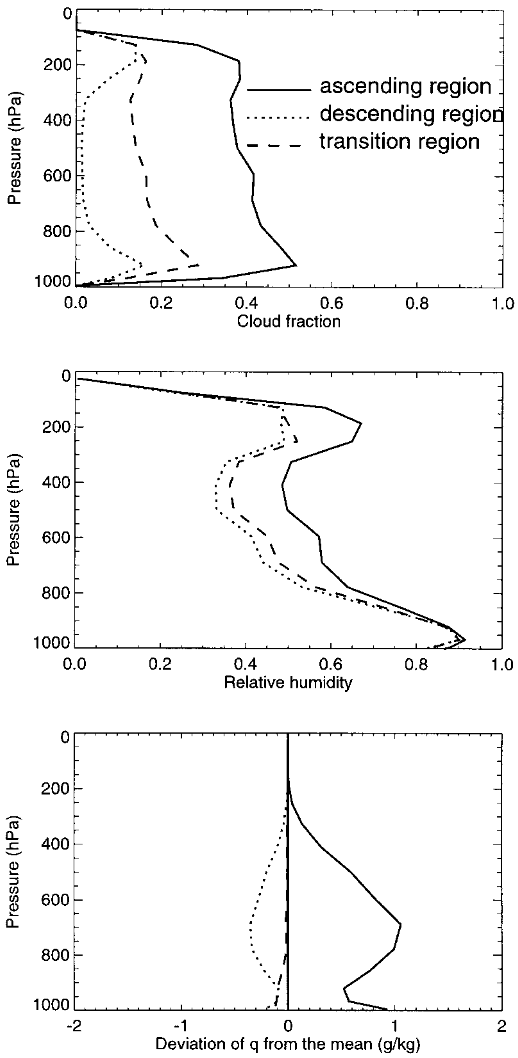


*Fig. 6.* Vertical profiles of vertical velocity, relative humidity and specific humidity (deviation from the domain mean) in upward motion, downward motion and transition regimes, stratified according to vertical velocity at 600 hPa.

and Houze, 1997; Sui et al., 1997). As a result, the cloud area also undergoes a similar diurnal variation. Fu et al. (1990) showed that there is a maximum in deep convective cloud cover in the early morning and a maximum in mesoscale anvil cloud cover in the late afternoon. Mapes and Houze (1993) found that the coldest cloud areas in organized cloud clusters reach a maximum before dawn and decreases throughout the day, while modestly cold cloud areas reach a maximum in the afternoon.

Fig. 7 demonstrates the diurnal variation of the cloud population and area for all deep clouds as well as MCSs from the model and observations of BR. Here the number and area are normalized by the maximum of each cloud type within the 24-h period to emphasize the diurnal variation. Note that the model output is four times a day whereas the satellite observations are available hourly. The total number of deep convective systems shows a slight maximum at noon in the model while the observations show a maximum before dawn and a secondary maximum in the afternoon. Noting that the cloud number is dominated by small clouds and that the model undersimulates small clouds, it is not surprising that the model does not simulate well the diurnal variation of the total cloud number for deep convective clouds. For MCSs the observed pre-dawn maximum in cloud number is reasonably well reproduced by the model, although the amplitude of the diurnal variation is less than observed. The modeled total area for all deep clouds exhibits a maximum in the early morning, in agreement with the satellite observations. Same as for the total number population, the late afternoon secondary maximum in cloud area is missing in the model. The area of the modeled MCSs has a primary maximum in the early morning and a weak secondary maximum in late afternoon, in qualitative agreement with the satellite observations. This suggests that the missing afternoon peak in cloud area is mostly from non-MCS type of deep convective clouds. To see if the coldest cloud systems in the model exhibit a single peak in the early morning, as observed by Mapes and Houze (1993), we isolated these cloud systems from the MCSs in the model. From Fig. 7, it is clear that the areas of the very cold cores of the MCSs (areas with cloud top temperature $<219$ K) reach a maximum in the early morning and decrease as the day progresses, in agreement with Mapes and Houze (1993).

The diurnal variation of the population and area for the mid-level and low clouds is shown in Fig. 8. The observed mid-level cloud population shows two maxima, one in the early morning and one in the afternoon, similar to the deep cloud population. The observed low cloud population

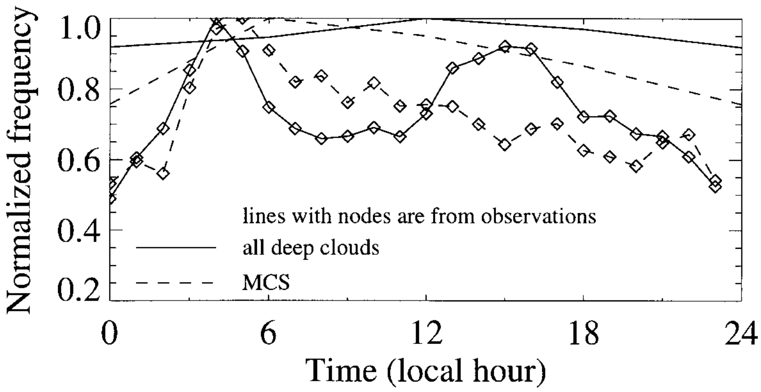


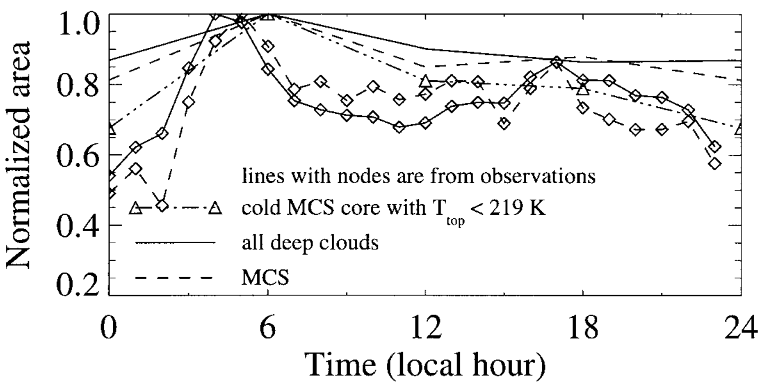


*Fig. 7.* Diurnal variation of number and area of deep clouds normalized by the maximum number of these clouds across the 24-h bins.

shows a single peak in the early morning and then decreases throughout the day. The diurnal variation of cloud number for both these two cloud types is poorly simulated in the model, which shows a minimum during the day and a maximum at midnight. The diurnal variation of the normalized cloud area for both the mid-level and low clouds from the observations shows a primary maximum in the early morning and a secondary maximum in the early evening. A broad minimum is observed during the day. This minimum is qualitatively simulated in the model. However, at midnight the model shows a maximum instead of the observed minimum.

Associated with the diurnal variation in convection and clouds, there is also a diurnal variation in the atmospheric thermodynamic state. Fig. 9 shows the domain averaged deviation of temperature and specific humidity from the daily mean for both the model and the ECMWF reanalysis. The diurnal variation of temperature from ECMWF shows that the troposphere is colder at night and warmer during the day. The same diurnal variation of temperature was documented by Sui et al. (1997) during TOGA COARE. The model simulates this diurnal cycle very well. The diurnal variation of the specific humidity shows that the atmosphere is significantly moister at midnight and drier in the early morning and evening. At local noon, the lower troposphere is slightly moister except near the surface where the air is drier. This diurnal variation is poorly simu-

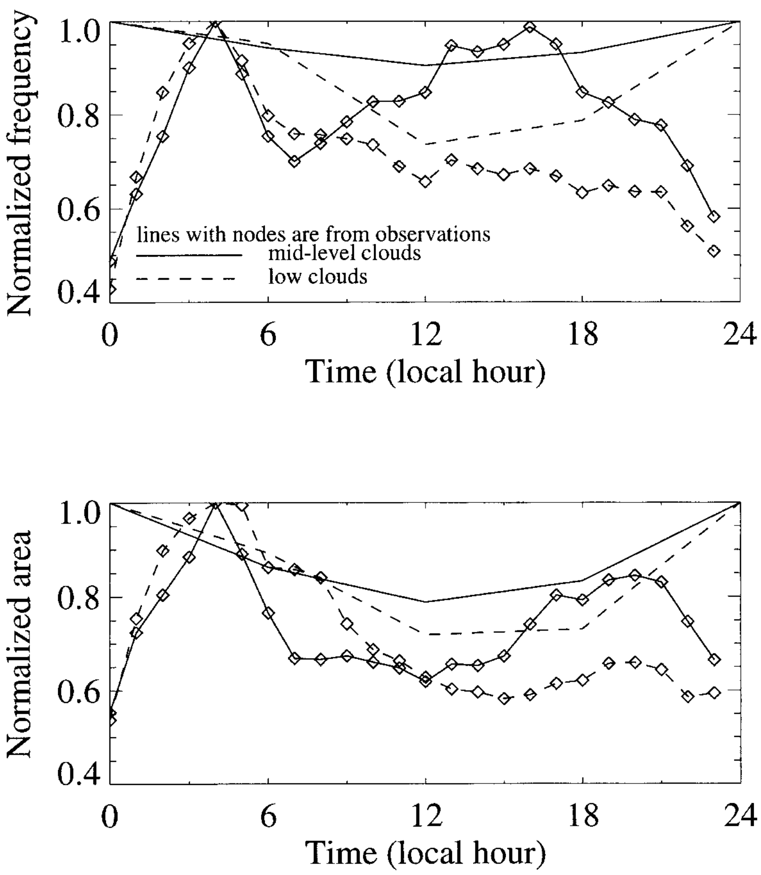


*Fig. 8.* Same as Fig. 7, but for mid-level and low clouds.

lated in the model. For instance, the model atmosphere at midnight is drier instead of moister compared to the other times of the day. The opposite is true at 6 a.m. local time. Also, near the surface the reanalysis shows the largest diurnal variation whereas the model diurnal variation is insignificant. The poor simulation of the moisture field reflects the difficulty in simulating the moisture field in numerical models.

## 5. Summary and discussions

The cloud classification algorithm by Boer and Ramanathan (1997) is applied to the cloud fields from a regional model in the tropical central and western Pacific region. It is shown that the area contribution from different types of the model clouds to the total cloud cover is in good agreement with satellite observations. However, both the number population and area of the relatively smaller clouds are under-simulated compared to the observations. On the other hand, the simulated numbers and cloud cover of large convective systems, in particular MCSs, as functions of the cloud scale are in very good agreement with the satellite observations. The statistical properties of the simulated low clouds are also in good agreement with the observations. It is also shown that the model cloud liquid water path, which is important for cloud radiative effects, precipitation and surface air–sea fluxes vary considerably with cloud type as well as cloud scale. These results are directly relevant to the effects of cloud systems on the surface energy budget and hydrological cycle.

We also examined the diurnal cycle of convec-

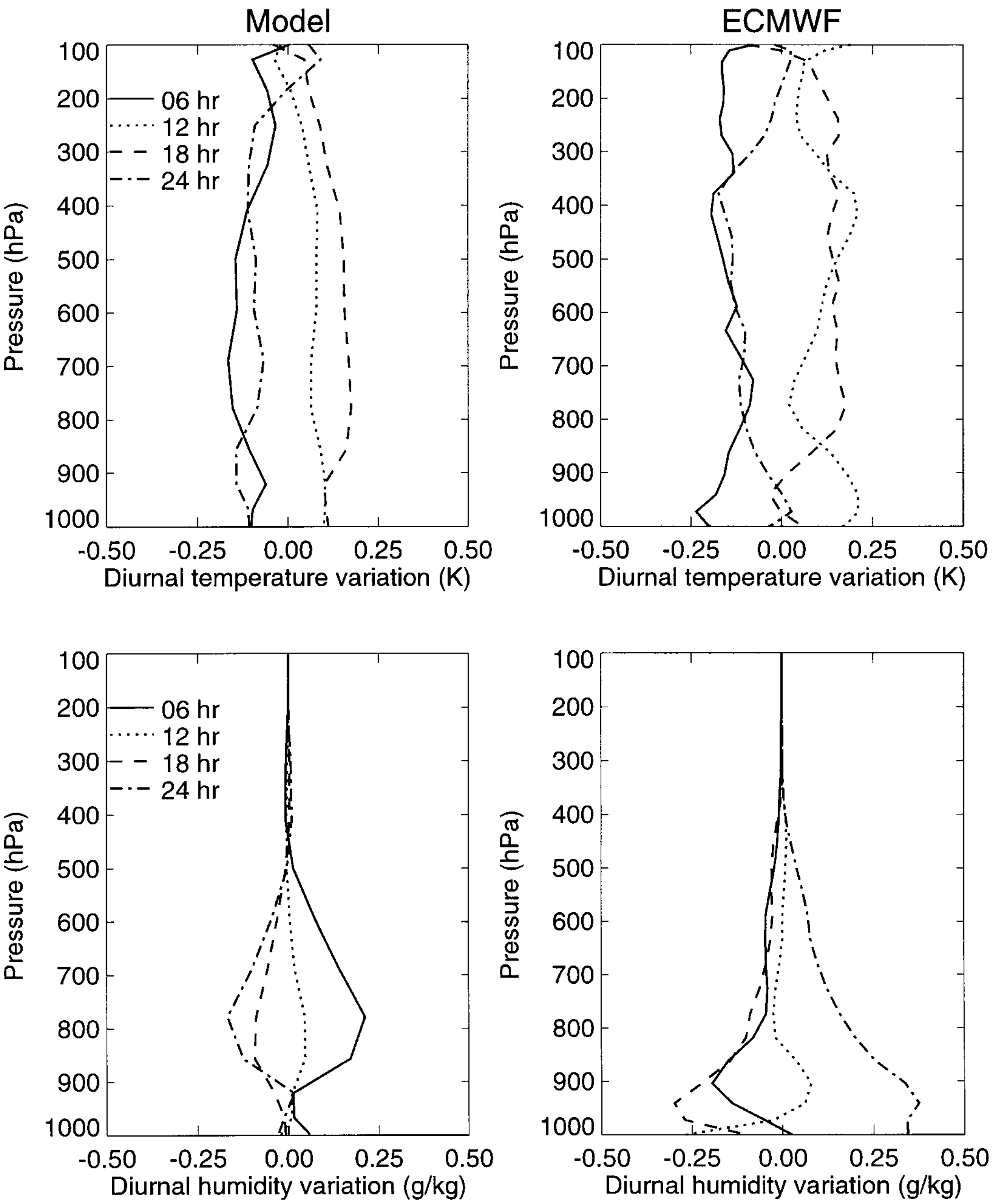


*Fig. 9.* Deviation of temperature and specific humidity from the daily mean averaged over the model domain for model output and ECMWF reanalysis.

tion and clouds, and the associated atmospheric thermodynamic states. It is shown that the diurnal variation of the number and area of the mesoscale convective systems is reasonably well simulated compared to the satellite observations. The primary maximum of cloud area in the early morning for deep clouds as a whole is also reasonably well simulated. However, the model fails to reproduce the diurnal variation of the number of deep clouds. The diurnal variation of temperature in the model compares well with the ECMWF reanalysis. The atmosphere is warmer during the day and colder at night. On the other hand, the diurnal variation of the moisture field is poorly simulated in the model. In the mid- and lower troposphere, the ECMWF reanalysis shows a moister atmosphere at midnight and a drier atmosphere in the morning, whereas the model atmosphere is drier at midnight and moister in the morning. Near the surface the observed diurnal cycle in the moisture field is almost completely missing in the model.

The most significant deficiency in the model simulated cloud statistics is that cloud population and area contribution to the total cloud cover at the lower end of the cloud size spectrum are under represented for both deep and mid-level convective cloud systems. The unsatisfactory simulation of the diurnal cycle of some cloud types may also be related to it. How is this deficiency related to cloud parameterization, and how can it be improved? While this is beyond the scope of this paper, here we offer some discussions on some possible approaches one can take. Note that large convective cloud systems, particularly MCSs are well simulated in both number and area distribution with respect to cloud size. It is the simulation of the relatively smaller clouds ($<10^5$ km$^2$ in area) that is more problematic. One possible area to look for improvement is the interaction between convection and the stratiform/anvil clouds in the model. The cloud parameterization scheme of Sundqvist et al. (1989) makes use of a modified Kuo (1974) scheme to parameterize convection. It allows anvils to develop from convection if the cloud top temperature is $<253$ K. Convection occurs when both the low-level moisture convergence and static stability criteria are met. The low-level convergence is closely connected to the representation of the dynamic processes in the model, which are affected by such factors as horizontal resolution and numerical damping. The damping used in the model is such that almost all of the 2-grid waves and a significant part of the 4-grid waves are filtered out, making it unfavorable for low level convergence, thus convection and clouds on such scales. Use of a stability dependent convective parameterization scheme such as Zhang and McFarlane (1995) may alleviate the problem since it is not constrained by the low level convergence. Another area in association with the convection and stratiform cloud interaction is the treatment of anvils. Anvils are treated as stratiform clouds, including their microphysical processes and the relative humidity threshold for cloud formation. In regions of relatively small convective cloud systems, relative humidity is low (Fig. 5), resulting in under-prediction of the anvil cloud cover. Lowering the relative humidity threshold for cloud formation can effectively increase the anvil cloud cover (Sigg, 1995). However, this would create too much cloud cover for large cloud systems. Apparently choosing a right relative humidity threshold is a complex issue. Another factor may be the treatment of hydrometeor re-evaporation in the model. Evaporation of hydrometeor is an important source of water vapor in the atmosphere, therefore directly affects the formation and maintenance of the cloud systems. Evaporation of precipitating water and cloud water/ice increases the environmental humidity, which increases both the convective and stratiform cloud cover. From Fig. 5, the relative humidity for small cloud systems is significantly less than for large cloud systems. Correspondingly, cloud cover is also small. Allowing for enhanced evaporation at low relative humidity probably will help alleviate the problem of under-simulating small clouds by the model.

This study is the first attempt to use a Lagrangian cloud classification algorithm to validate the simulation of the cloud fields by a high-resolution regional model. More research is needed to estimate the sensitivity of the cloud statistics to various assumptions in the algorithm and the limitations of the model. For instance, a geometric temperature field $T_g$ is used as input to the cloud classification algorithm in the current study. Alternatively, an effective brightness temperature field can be obtained using outgoing long-wave radiation using some empirical relationships. However, the outgoing long-wave radiation field in the current version of the model may not be accurate enough for this purpose because of the crude radiation parameterization. One possible extension of the current study is to use a more comprehensive radiation parameterization. This together with the aforementioned convection/anvil interaction will be the subject of future study.

## 6. Acknowledgments

This research was supported by the Environmental Science Division of US Department of Energy under grant DEFG 0391 ER 61198 (GJZ). The leading author (GJZ) would like to thank Professor Hilding Sundqvist for making the HIRLAM model available to him.


REFERENCES


Boer, E. and Ramanathan, V. 1997. Lagrangian approach for deriving cloud characteristics from satellite observations and its implications to cloud parameterization. *J. Geophys. Res.* **102**, 21,383–21,399.

Chen, S. S. and Houze Jr, R. A. 1997. Diurnal variation and life-cycle of deep convective systems over the tropical Pacific warm pool. *Quart. J. Roy. Meteo. Soc.* **123B**, 357–388.

Del Genio, A. D., Yao, M. S., Kovari, W. and Lo, K. K. W. 1996. A prognostic cloud water parameterization for global climate models. *J. Climate* **9**, 270–304.

Fu, R., Del Genio, A. D. and Rossow, W. B. 1990. Behavior of deep convective clouds in the tropical Pacific from ISCCP radiances. *J. Climate* **3**, 1129–1152.

Huang, X. Y. and Sundqvist, H. 1993. Initialization of cloud water content and cloud cover for numerical prediction models. *Mon. Wea. Rev.* **121**, 2719–2726.

Karlsson, K.-G. 1996. Validation of modelled cloudiness using satellite-estimated cloud climatologies. *Tellus* **48A**, 767–785.

Kuo, H. L. 1974. Further studies parameterization of the influence of cumulus convection on large-scale flow. *J. Atmos. Sci.* **31**, 1232–1240.

Louis, J. F. 1979. A parametric model of vertical eddy fluxes in the atmosphere. *Boundary Layer Meteor.* **17**, 187–202.

Liu, G., Curry, J. A. and Sheu, R. S. 1995. Classification of clouds over the western equatorial Pacific Ocean using combined infrared and microwave satellite data. *J. Geophys. Res.* **100**, 13,811–13,826.

Mapes, B. E. and Houze Jr, R. A. 1993. Cloud clusters and superclusters over the oceanic warm pool. *Mon. Wea. Rev.* **121**, 1398–1415.

Rind, D. E., Chiou, W., Chu, W., Larsen, J., Oltmans, S., Lerner, J., McCormick, M. P. and McMaster, L. 1991. Positive water vapor feedback in climate models confirmed by satellite data. *Nature* **349**, 500–503.

Russ, J. C. 1992. *The image processing handbook*. CRC Press, Inc., Boca Raton, 322 pp.

Savijärvi, H. 1991. Fast radiation parameterization schemes foe mesoscale and short-range forecast models. *J. Appl. Meteor*. **29**, 437–447.

Sigg, R. 1995. Anvil formation in a convective parameterization scheme. Report DM-71, Dept. of Meteorology, Stockholm University, Sweden. Available from author.

Soden, B. J. and Fu, R. 1995. A satellite analysis of deep convection, upper-tropospheric humidity, and the greenhouse effect. *J. Climate* **8**, 2333–2351.

Sui, C. H., Lau, K. M., Takayabu, Y. N. and Short, D. A. 1997. Diurnal variations in tropical oceanic cumulus convection during TOGA COARE. *J. Atmos. Sci.* **54**, 639–655.

Sun, D.-Z. and Lindzen, R. S. 1993. Distribution of tropical tropospheric water vapor. *J. Atmos. Sci.* **50**, 1643–1660.

Sundqvist, H., Berge, E. and Kristjansson, J. E. 1989. Condensation and cloud parameterization studies with a mesoscale numerical weather prediction model. *Mon. Wea. Rev.* **117**, 1641–1657.

Yu, W., Garand, L. and Dastoor, A. P. 1997. Evaluation of model clouds and radiation at 100 km scale using GOES data. *Tellus* **49A**, 246–262.

Zhang, G. J. and McFarlane, N. A. 1995. Sensitivity of climate simulations to the parameterization of cumulus convection in the Canadian Climate Centre general circulation model. *Atmos.-Ocean* **33**, 407–446.

Zhang, G. J., Ramanathan, V. and McPhaden, M. J. 1995. Convection-evaporation feedback in the equatorial Pacific. *J. Climate* **8**, 3040–3051.